Chinese Journal of Natural Medicines

***Selaginella tamariscina* extract and amentoflavone ameliorate UVB-induced skin aging via AMPK activation**

Lu Wang, Mingjie Li, Zhao Zhang, Hairan Fan, Yahui Mi, Wei Shi, Haimin Kuai, Xiaolong Hu, Fei Xiong, Hao Wang, Peng Shu, Rong Wang

Citation: Lu Wang, Mingjie Li, Zhao Zhang, Hairan Fan, Yahui Mi, Wei Shi, Haimin Kuai, Xiaolong Hu, Fei Xiong, Hao Wang, Peng Shu, Rong Wang, *Selaginella tamariscina* extract and amentoflavone ameliorate UVB-induced skin aging *via* AMPK activation, Chinese Journal of Natural Medicines, 2026, 24(4), 470-484. doi: 10.1016/S1875-5364(26)61116-8.

View online: https://doi.org/10.1016/S1875-5364(26)61116-8

Chinese Journal of Natural Medicines 24 (2026) 470-484

Contents lists available at ScienceDirect

Chinese Journal of Natural Medicines

journal homepage: www.cjnmcpu.com/

Original article

Selaginella tamariscina extract and amentoflavone ameliorate UVB-induced skin aging *via* AMPK activation

Lu Wang[a,Δ], Mingjie Li[b,Δ], Zhao Zhang[a], Hairan Fan[a], Yahui Mi[a], Wei Shi[a], Haimin Kuai[a], Xiaolong Hu[a], Fei Xiong[c], Hao Wang[a,*], Peng Shu[b,*], Rong Wang[a,*]

[a] *State Key Laboratory of Natural Medicines, School of Traditional Chinese Pharmacy, China Pharmaceutical University, Nanjing 211198, China*
[b] *HBN Research Institute and Biological Laboratory, Shenzhen Hujia Technology Co., Ltd., Shenzhen 518000, China*
[c] *State Key Laboratory of Bioelectronics, School of Biological Science and Medical Engineering, Southeast University, Nanjing 210009, China*

ARTICLE INFO

Article history:
Received 27 May 2025
Revised 3 August 2025
Accepted 7 August 2025
Available online 20 April 2026

Keywords:
Selaginella tamariscina
Amentoflavone
Photoaging
Autophagy
AMPK

ABSTRACT

Ultraviolet (UV) exposure accelerates skin aging and increases the risk of skin-related diseases. Amentoflavone (AMF), the major compound isolated from *Selaginella tamariscina*, exhibits potent antioxidant and anti-inflammatory activities. This study aimed to investigate the therapeutic effects and mechanisms of *S. tamariscina* extract (STE) and AMF on UVB-induced skin photoaging. *In vitro* and *in vivo* photoaging models were established to evaluate the protective effects of STE and AMF. The therapeutic target of AMF was identified using network pharmacology, bioinformatic analysis, and molecular docking. *In vitro*, STE significantly reduced UVB-induced oxidative stress, inflammation, and apoptosis. *In vivo*, both STE and AMF effectively mitigated UVB-induced skin injury. Mechanistically, AMF directly interacted with AMP-activated protein kinase (AMPK), thereby promoting autophagy and protecting cells from UVB-induced damage. In conclusion, STE and its active compound AMF alleviate UVB-induced photoaging *via* activation of the AMPK signaling pathway, supporting their potential use in skin photoaging therapy.

1. Introduction

The skin serves as the primary barrier between the body and the external environment, playing a vital role in protection, temperature regulation, and metabolic exchange [1]. Skin aging results from the combined effects of intrinsic (genetic) and extrinsic (environmental) factors, leading to both structural changes and functional decline [2]. Among these, ultraviolet (UV) radiation, particularly UVB, is the predominant environmental factor contributing to skin aging, accounting for over 80% of the visible facial aging [3, 4]. UVB-induced oxidative stress damages cellular macromolecules, triggers inflammation, and promotes collagen degradation, ultimately leading to skin loosening, roughness, and capillary dilation [5-7].

AMP-activated protein kinase (AMPK), a crucial energy sensor, plays a significant role in aging regulation [8]. AMPK activation has been associated with lifespan extension; for example, increased AMPK expression prolongs lifespan by 13% in *C. elegans* [9]. Autophagy, a key downstream process of AMPK, maintains cellular homeostasis by degrading damaged proteins and organelles while adapting cellular metabolism to stress conditions. Mechanistically, AMPK activates autophagy through phosphorylation of ULK1 and inhibition of the mTOR pathway [10]. Enhancing autophagy has been shown to delay aging and promote longevity [11]. Studies have shown that UVB exposure can inhibit autophagy in human epidermoid carcinoma A431 cells [12]. Specifically, UVB exposure activates the mTOR pathway, which suppresses autophagy and accelerates photoaging [13]. It has been shown that rhFGF21 can protect epidermal cells from UVB-induced apoptosis by activating AMPK-mediated autophagy, underscoring the critical roles of AMPK and autophagy in combating UVB-induced photoaging [14].

Selaginella tamariscina (P. Beauv.) Spring, mainly distributed in the southern area of Changjiang River in China, is widely utilized in traditional Chinese medicine for the treatment of blood stasis and carbuncles. Recent studies have highlighted its broad spectrum of pharmacological activities, including anti-inflammatory and anti-tumor effects [15, 16]. In Korea, *S. tamariscina* is also widely used in cosmetic formulations [17]. *S. tamariscina* reduces the production of inflammatory mediators and pro-inflammatory cytokines in a dose-dependent manner in LPS-induced RAW 264.7 cells, demonstrating its anti-inflammatory potential [18]. Furthermore, biflavonoids from *S. tamariscina* downregulate the expression of matrix metalloproteinases (MMPs), which are zresponsible for degrading extracellular matrix components such as collagen and elastin in skin fibroblasts [19, 20]. In addition, the abundant biflavonoid in *S. tamariscina*, amentoflavone (AMF) significantly attenuates the UVB-induced upregulation of Lamin A and phospho-H2AX expression [21]. These investigations suggest that *S. tamariscina* and AMF demonstrate potential in mitigating skin photoaging. However, the anti-photoaging effects of *S. tamariscina* extract (STE) and AMF, along with their pharmacological basis, underlying mechanisms, and molecular targets, remain to

* Corresponding author.
E-mail addresses: wanghao@cpu.edu.cn (H. Wang); shupeng@hbn.cn (S. Peng); wangrong@cpu.edu.cn (R. Wang)
Δ These authors contributed equally to this work.

https://doi.org/10.1016/S1875-5364(26)61116-8

be elucidated.

In this study, both *in vitro* and *in vivo* models were utilized to evaluate the protective effects of STE and AMF against UVB-induced photoaging in keratinocytes and mouse skin. Furthermore, the molecular mechanisms underlying the anti-photoaging effects of AMF were investigated. These findings suggest that both STE and AMF may serve as potential anti-photoaging agents, providing a novel theoretical foundation for the development of treatments targeting skin photoaging.

2. Material and methods

2.1. Extraction and determination of STE

The whole herb of *S. tamariscina*, purchased from Bozhou City (China) in August 2023, was identified as *Selaginella tamariscina* (P. Beauv.) Spring by Professor Hao Wang of China Pharmaceutical University. The specimens were deposited in the Laboratory of Natural Medicinal Chemistry, China Pharmaceutical University (voucher specimen number: 2023-0830). The pulverized dried herb (200 g) was extracted with 80% ethanol (2000 mL) under reflux at 90 °C for 2 h, and this procedure was repeated twice. The filtrates were combined and concentrated to obtain a crude extract. The residue was dissolved and suspended in 200 mL of 50% EtOH, stored at 5 °C for 12 h, and then subjected to suction filtration. This water precipitation process was repeated twice. Finally, the resulting precipitate was vacuum-dried at 60 °C to obtainSTE (4.3 g). For analysis, 0.1 g of STE powder was dissolved in 50 mL of methanol, and the solution was filtered through a 0.22 μm microporous membrane. For reference standard solutions, 5.2 mg of AMF, 4.9 mg of hinokiflavone, and 5.1 mg of isocryptomerin were each dissolved in 10 mL of methanol. HPLC analysis was performedon an Agilent 1260 series HPLC-DAD system (Agilent, Waldbronn, Germany) using a Shimadzu ODS column (250 mm × 4.6 mm, 5 μm). The mobile phase consisted of water containing 0.1% phosphoric acid (A) and acetonitrile (B), with the following gradient elution: 0–15 min, 30% B; 15–25 min, 30%–50% B; 25–35 min, 50%–70% B; 35–50 min, 70%–90% B. The detection wavelength was set at 330 nm, the column temperature was maintained at 30 °C, the injection volume was 10 μL, and the flow rate was 1.0 mL·min^{-1}. All test compounds were isolated from *S. tamariscina* in our laboratory (purity > 95%).

2.2. Cell culture

HaCaT cells were purchased from the Cell Resource Center of the Shanghai Institutes for Biological Sciences, Chinese Academy of Sciences (Shanghai, China). The cells were cultured in high-glucose DMEM (KeyGEN, China, #KGL1206-500), with 10% fetal bovine serum (FBS) (Sigma–Aldrich, St. Louis, MO, USA) added to the medium. HaCaT cells were incubated at 37 °C in an atmosphere with 5% CO_2.

2.3. Cell photoaging model

HaCaT cells were pre-treated with different concentrations of STE (5 and 10 μg·mL^{-1}), AMF (3 and 6 μmol·L^{-1}), Vitamin E (VE) (10 μmol·L^{-1}) (Huazhong Pharmceutical Co., Ltd., China), Compound C (CC) (10 μmol·L^{-1}) (Yuanye Bio-Technology Co., Ltd., China, #T88495) or 3-Methyladenine (3-MA, 1 mmol·L^{-1}) (MedChemExpress, USA, #HY-19312) for 4 h, after which the medium was discarded. The cells were then exposed to UVB irradiation (150 mJ·cm^{-2}). Following UVB exposure, high-glucose DMEM supplemented with 10% FBS and the corresponding treatments (STE, AMF, VE, or CC) was added, and the cells were incubated at 37 °C in a 5% CO_2 incubator for 24 h. Control cells were not exposed to UVB irradiation and received no drug treatment.

2.4. Cell viability assays

HaCaT cells were seeded into a 96-well plate (1 × 10^4 cells/well). Following the protocol of the manufacturer, a CCK-8 assay kit (Beyotime, China, #C0037) was used to detect the cytotoxicity of STE and AMF, as well as the protective effects of different concentrations of STE and AMF on the viability of HaCaT cells exposed to UVB radiation. CCK-8 reagent was added to each well and incubated at 37 °C for 4 h, and the cell quantity was estimated by measuring absorbance at 450 nm using a microplate reader (TECAN Sunrise, Switzerland).

2.5. 5-Ethynyl-2′-deoxyuridine (EdU) growth assay

HaCaT cells were seeded into a 96-well plate (1 × 10^4 cells/well), and an EdU cell proliferation assay kit (Beyotime, China, #C0071S) was employed to evaluate the effects of different treatments on cell proliferation. The cells were incubated with 50 μmol·L^{-1} EdU for 2 h, followed by fixation, permeabilization, and EdU staining. Subsequently, the nuclei were stained with Hoechst 33342 (Beyotime, China, #C1022, 1∶1000), and the percentage of EdU-positive cells was determined using an inverted fluorescence microscope (Nikon, Japan).

2.6. Cell apoptosis detection

After treatment with different concentrations of STE, AMF, or VE, approximately 1 × 10^6 cells were collected. According to the instructions of the kit (KeyGEN, China, #KGA1102-100), 5 μL of Annexin V-FITC was added to the cell suspension and mixed thoroughly, followed by the addition of 5 μL of propidium iodide. The mixture was incubated in the dark at room temperature for 10 min. Subsequently, the samples were analyzed using flow cytometry (BD Accuri, USA).

2.7. ShRNA and AMPK plasmid transient transfection

Lentiviral particles containing scramble shRNA (sc-shRNA) or shRNA targeting AMPKα1 were synthesized, verified, and provided by Qingke Biotechnology Co., Ltd. (Beijing, China). The hairpin sequence for AMPKα1 was 5′-CTCCAAGACCAGGAAGTCATACAATAGAA-3′. For transient transfection, AMPK or sc-shRNA was introduced into the corresponding wells using Lipofectamine™ 3000 reagent following the manufacturer's instructions. Following transfection, HaCaT cells were treated with AMF (6 μmol·L^{-1}) or metformin (MET) (10 μmol·L^{-1}) (MedChemExpress, USA, #HY-B0627) for 4 h. The following steps were the same as those described above for the cell photoaging model (Section 2.3).

2.8. UVB-irradiated skin photoaging model and treatment in ICR mice

ICR mice (male, 7–8 weeks old, weighing 21–23 g) were purchased from Shanghai Slac Laboratory Animal Co., Ltd. (Shanghai, China). They were maintained under a 12 h light/dark cycle with free access to food and water. All animal experiments were approved by the Institutional Animal Care and Use Committee at China Pharmaceutical University (No. SYXK2021-0011). After the dorsal hair of the mice was shaved, the mice were irradiated with a UVB lamp (YIXIAN, China) placed 2 cm above the dorsal skin every other day for 6 weeks. The radiation dose during the first three weeks was set to the minimal erythema dose (100 mJ·cm^{-2}) and was increased to 200 mJ·cm^{-2} from weeks 3 to 6. For treat-

ment, the mice were randomly divided into seven groups (n = 7): a) control group: no drug treatment and no UVB irradiation; b) UVB group: UVB irradiation without drug treatment; c) VE treatment group: UVB irradiation with daily topical application of VE (2%, Institute of Dermatology, Chinese Academy of Medical Sciences); d) low-dose STE group: UVB irradiation with daily topical application of STE (1%); e) high-dose STE group: UVB irradiation with daily topical application of STE (2%); f) low-dose AMF group: UVB irradiation with daily topical application of AMF (0.3%); g) high-dose AMF group: UVB irradiation with daily topical application of AMF (1.2%).

2.9. Acute skin toxicity test

All mice were anesthetized with isoflurane to facilitate dorsal hair removal. On the day before irradiation, the hair was removed with a shaver followed by depilatory cream, and the exposed dorsal skin area (about 3 cm × 3 cm) was cleaned and dried. Mice with pre-existing skin abnormalities were excluded. The animals were randomly assigned to three groups (n = 5): control group, STE group (2%), and AMF group (0.6%). Each group included intact-skin and damaged-skin subgroups. The designated skin area was treated with blank matrix, STE, or AMF ointment, covered with gauze, and secured with elastic bandages. After 24 h of treatment, the formulations were removed from the dorsal skin. Daily monitoring was performed until day 7, including assessment of general condition, body weight, and skin appearance. On day 7, dorsal skin was collected, fixed in paraformaldehyde, and examined histologically by H&E staining.

2.10. Ex-vivo drug permeation studies

The Franz diffusion cell method was used to evaluate skin permeability [22]. Five 8-week-old male ICR mice were anesthetized and sacrificed by cervical dislocation. Dorsal hair was removed with depilatory cream, and the underlying connective tissue and subcutaneous fat were carefully excised. The isolated skin was mounted on the diffusion chamber, and 2 mL of AMF emulsion (0.6%) was added to the donor compartment. The effective diffusion area was 2.8 cm^2, and the receptor volume was 7 mL of 20% ethanol in PBS (pH 7.4). During the experiment, the system was maintained at 37 °C under constant magnetic stirring (100 r·min^{-1}). At predetermined time points (0, 1, 2, 4, 6, 8, 10, 12, and 24 h), 0.4 mL of receptor fluid was withdrawn and replaced with an equal volume of fresh buffer. The cumulative penetration amount (Q_n, μg·cm^{-2}) was then calculated using the following equation:

$$Q_n = (C_n \times V_0 + \sum_{i=1}^{n-1} C_i \times V_i)/Ac$$

In this equation, c_i and c_n represent the AMF concentrations (μg·mL^{-1}) determined at the i-th and n-th sampling points, respectively; A denotes the effective diffusion area; V_0 is the total volume of the receptor solution; and V_i corresponds to the sampling volume.

2.11. Stability studies

The stability of AMF was evaluated in accordance with General Rule 9001, Part IV of the 2020 Chinese Pharmacopoeia, which outlines the principles for stability testing of raw materials and preparations [23]. Stress conditions included elevated temperature (60 ± 2 °C), high humidity (25 °C, 90% ± 5% relative humidity), and intense light exposure (4500 ± 500 lux). Samples were examined at 0, 5, and 10 days for key quality attributes, including physical appearance and AMF content, to comprehensively assess AMF stability.

2.12. Superoxide dismutase (SOD) assay

HaCaT cells and mouse skin tissues were collected after the corresponding treatments. A WST-8 superoxide dismutase assay kit (Beyotime, China, #S0101S) was used to measure SOD activity according to the guidelines of the manufacturer. The colorimetric reaction was performed in a 96-well plate, and absorbance was measured at 450 nm using a microplate reader (TECAN Sunrise, Switzerland).

2.13. Malondialdehyde (MDA) assay

The MDA content assay kit (Beyotime, China, #S0131S) was used according to the manufacturer's instructions. Proteins were extracted from treated HaCaT cells and mouse skin tissues as required by the kit. MDA detection working solution was then added, and after heating and centrifugation, the supernatant was transferred to a 96-well plate. Absorbance was measured at 530 nm using a microplate reader (TECAN Sunrise, Switzerland).

2.14. RNA extraction and real-time RT-PCR

Total RNA was extracted from samples using Trizol reagent (Invitrogen, USA, #155960-18). The isolated RNA was reverse-transcribed into complementary DNA (cDNA) using a cDNA synthesis kit (Vazyme Biotech, China, #R223). Quantitative PCR (qPCR) was performed using SYBR Green real-time PCR premix (Vazyme, China, #Q711), and relative quantification was carried out using the cycle threshold (Ct) method. Primer sequences are listed in Table S1.

2.15. Histological analysis

Dorsal skin was collected from mice after sacrifice, fixed in 4% paraformaldehyde, and embedded in paraffin for histopathological examination. Paraffin-embedded tissue blocks were sectioned at 5 μm using a rotary microtome. Sections were stained with H&E (Abcam, USA, #ab245880) and Masson's trichrome (Abcam, USA, #ab150686). Images were acquired using an upright microscope (Olympus, Japan).

2.16. Immunohistochemistry staining

For immunohistochemistry, tissue sections were dewaxed, hydrated, and permeabilized. Antigen retrieval was performed by heating the sections in 0.1 mol·L^{-1} citrate buffer (pH 6.0) at 95 °C for 30 min. Endogenous peroxidase activity was blocked with 3% hydrogen peroxide diluted in PBS. The sections were then incubated with 5% bovine serum albumin in PBS at room temperature for 1 h to block non-specific binding. Subsequently, the sections were incubated overnight at 4 °C with an anti-matrix metalloproteinase-3 (MMP-3) antibody (Affinity Biosciences, USA, #AF0217, 1:200), followed by staining and sealing. The samples were then examined under an upright fluorescence microscope (Olympus, Japan).

2.17. Immunofluorescence staining

Cells were immunofluorescently stained with primary antibodies against MMP-1 (Cell Signaling Technology, USA, #54376, 1∶200), TNF-α (Cell Signaling Technology, USA, #11948, 1∶200), IL-1β (Cell Signaling Technology, USA, #12703, 1∶200), IL-6 (Cell Signaling Technology, USA, #12912, 1∶200), MMP-2 (Cell Signaling Technology, USA, #40994, 1∶200), and COL1A1 (Cell Signaling Technology, USA, #72026, 1∶200) at 4 °C. After incubation with Alexa Fluor® 594-conjugated anti-rabbit IgG (Thermo Fisher Scientific, Waltham, MA, USA, #A21207; 1∶500) and Alexa

Fluor® 488-conjugated anti-rabbit IgG (Thermo Fisher Scientific, Waltham, MA, USA, #A-11008, 1∶500), 4',6-diamidino-2-phenylindole (DAPI, Southern Biotech, USA) was used for nuclear visualization. All images were captured with a laser scanning confocal microscope (LSCM) (Olympus, Japan).

2.18. Measurement of skin moisture content

To measure skin moisture content, dorsal skin samples were dried at 105 °C for 6 hours until a constant weight was reached. Moisture content (%) = (weight of fresh skin – weight of dry skin) / weight of fresh skin × 100.

2.19. Network pharmacology

Potential targets of AMF were predicted based on its chemical structure using the SwissTargetPrediction database. Photoaging-related targets were identified and validated using multiple databases, including Online Mendelian Inheritance in Man (OMIM), Therapeutic Target Database (TTD), Pharmacogenomics Knowledgebase (PharmGKB), Disease Target Network Database (DisGeNET), and DrugBank. The interaction network between AMF and photoaging-related targets was analyzed using the STRING database. In addition, Gene Ontology (GO) and Kyoto Encyclopedia of Genes and Genomes (KEGG) enrichment analyses of the identified targets were performed using the DAVID database. Finally, the bioavailability of AMF was predicted to evaluate its therapeutic potential.

2.20. Bioinformatic analyses with data from GeneExpression Omnibus (GEO) database

Single-cell RNA sequencing (scRNA-seq) data from publicly available GEO samples (GSE281449), including three old and three young samples, were analyzed using R and the Seurat package (version 4.3.0.1) to identify cellular subpopulations. The 10X Genomics scRNA-seq data were converted into Seurat objects. Quality control retained genes expressed in at least three cells and cells with at least 200 detected genes. Mitochondrial content was calculated using the PercentageFeatureSet function and restricted to below 25%. Gene expression was normalized using the NormalizeData function to reduce technical noise. The top 2000 highly variable genes were identified using the FindVariableFeatures function. Principal component analysis (PCA) was performed to reduce dimensionality and capture dominant biological signals. To correct for batch effects, data were integrated using the RunHarmony function from the Harmony R package based on PCA results. The DotPlot function in Seurat was used to visualize gene expression across subpopulations and identify key genes and their expression patterns across age groups.

2.21. Molecular docking

The X-ray crystal structure of AMPK (PDB: 4CFE) was obtained from the Protein Data Bank (https://www.rcsb.org/). The protein structure was optimized through hydrogen addition and water molecule removal, with the active site defined by the internal ligand in the Glide Generation module. The three-dimensional structure of AMF was prepared for docking using the Ligand Preparation module. Molecular docking was performed using the Ligand Interaction module of Discovery Studio 3.0 software.

2.22. Cellular thermal shift assay (CETSA) and isothermal dose-response fingerprint (ITDRF$_{CETSA}$)

HaCaT cells were incubated with AMF (10 μmol·L^{-1}) for 3 h, with the negative control group treated with an equal volume of DMSO. Subsequently, the cells were collected and evenly distributed into eight different 1.5 mL tubes, heated at designated temperatures (37 to 65 °C) for 3 min, and then lysed for protein extraction. The soluble proteins were analyzed by Western blot. For the ITDRF$_{CETSA}$ experiment, the same procedure was followed, except that cells were incubated with different concentrations of AMF (0–20 μmol·L^{-1}) at 53 °C.

2.23. Transmission electron microscopy

HaCaT cells treated with AMF or UVB were harvested and fixed in 2.5% glutaraldehyde for 2 h, followed by postfixation with osmium tetroxide. Samples were dehydrated through a graded ethanol series (50%–100%) and infiltrated with propylene oxide. The cells were then embedded in fresh epoxy resin, sectioned at a thickness of 350 nm, and stained with uranyl acetate and lead citrate. Ultrastructural observations were performed using a transmission electron microscope (JEM-1011, JEOL, Japan).

2.24. Double-labeled lentivirus mRFP-GFP-LC3 transfection

HaCaT cells were seeded in confocal Petri dishes and cultured for 24 h for attachment. Cells were then transfected with mRFP-GFP-LC3 lentivirus (Hanbio, Shanghai, China) according to the manufacturer's protocol, followed by AMF and UVB treatment. Nuclei were stained with Hoechst 33342.

2.25. Western blot analysis

HaCaT cells or mouse skin tissues were lysed using RIPA buffer (Beyotime, China, #P0013E) supplemented with protease inhibitor (Beyotime, China, #P1005). Proteins were separated on 10% SDS-PAGE gels (Beyotime, China, #P0014A-2bgs) and then transferred onto polyvinylidene difluoride membranes (Millipore Sigma, Germany). Membranes wer blocked with 5% skim milk at room temperature for 1 h and incubated with primary antibodies at 4 °C overnight. The next day, membranes were washed for 10 min with tris-buffered saline containing Tween 20 and then incubated at room temperature with HRP-conjugated secondary antibody (Cell Signaling Technology, USA, #7074P2, 1∶10 000). Immunoreactive bands were quantitatively analyzed using ImageJ software (NIH, Bethesda, MD, USA). Primary antibodies are provided in Table S2.

2.26. Statistical analysis

Data are presented as mean ± standard deviation (SD). All graphs and statistical analyses were performed using GraphPad Prism version 8 (GraphPad Software, San Diego, CA). Statistical analysis was performed using one-way analysis of variance (ANOVA) followed by Tukey's multiple comparison test, with $P < 0.05$ considered statistically significant.

3. Results

3.1. STE protects HaCaT cells from UVB-induced cell damage

UVB radiation inhibited HaCaT cell proliferation and induced photoaging in a dose-dependent manner. Specifically, exposure to 150 mJ·cm^{-2} of UVB significantly reduced HaCaT cell viability to approximately 50% (Supplementary Fig. S1A). Based on this result, a UVB dose of 150 mJ·cm^{-2} was selected for subsequent experiments. The cytotoxicity of STE in HaCaT cells was then evaluated, revealing that cell viability decreased when the STE concen-

tration exceeded 100 μg·mL^{-1} (Supplementary Fig. S1B). Accordingly, STE concentrations of 5 and 10 μg·mL^{-1} were chosen for further studies. The efficacy results showed that STE effectively mitigated UVB-induced effects by enhancing cell proliferation and preserving normal cellular morphology (Figs. 1A–1D). Furthermore, flow cytometry analysis revealed that apoptosis was significantly increased in HaCaT cells after UVB exposure compared with the control group, while STE treatment markedly reduced UVB-induced apoptosis (Figs. 1E–1F). These results indicate that STE exerts protective effects against UVB-induced cellular damage in HaCaT cells.

3.2. Component analysis of STE

The extract was analyzed by HPLC. As shown in Supplementary Figs. S2–S11, three active components, AMF, hinokiflavone, and isocryptomerin, were quantified in= STE. Their contents were 301.2, 20.5, and 6.5 mg·g^{-1}, respectively, with AMF being the most abundant component. Among these compounds, AMF showed the strongest protective effect against UVB-induced cellular damage and was therefore selected for further investigation (Supplementary Fig. S12).

3.3. STE and AMF protect HaCaT cells from UVB-induced cellular aging

Cytotoxicity assays revealed that AMF did not significantly affect HaCaT cell viability at concentrations below 10 μmol·L^{-1} (Supplementary Fig. S1C). HPLC-based quantification further revealed that the AMF content within 5 and 10 μg·mL^{-1} STE corresponded approximately to 3 and 6 μmol·L^{-1} of pure AMF, respectively. These concentrations were therefore selected for subsequent experiments to allow direct comparison with STE and to determine whether the protective effects of STE were primarily attributable to AMF.

During senescence, cells lose proliferative capacity, undergo cell cycle arrest, and show increased expression of cell cycle regulatory proteins [24,25]. Senescence is also accompanied by the senescence-associated secretory phenotype, characterized by increased secretion of MMPs [26]. Our data showed that UVB irradiation significantly increased the mRNA expression of *p21*, *p16*, *MMP-1*, and *MMP-9* in HaCaT cells. STE and AMF dose-dependently suppressed these changes, suggesting protective effects against UVB-induced photoaging (Figs. 2A–2D). Immunofluorescence staining further showed that STE and AMF markedly reduced UVB-induced MMP-1 overexpression in HaCaT cells (Figs. 2E–2F). Western blot analysis confirmed that the protein levels of p21, p16, and MMP-1 were significantly increased in the model group (Figs. 2G–2I), consistent with the mRNA results. STE and AMF markedly reversed these UVB-induced changes. In addition, Western blot analysis showed an increased Bcl-2/Bax ratio after STE and AMF treatment compared with UVB treatment alone (Figs. 2G and 2J). These results suggest that STE and AMF effectively protect HaCaT cells from UVB-induced cellular aging.

3.4. STE and AMF degrade inflammation in vitro

Oxidative stress is an early event in photoaging [4]. UVB expos-

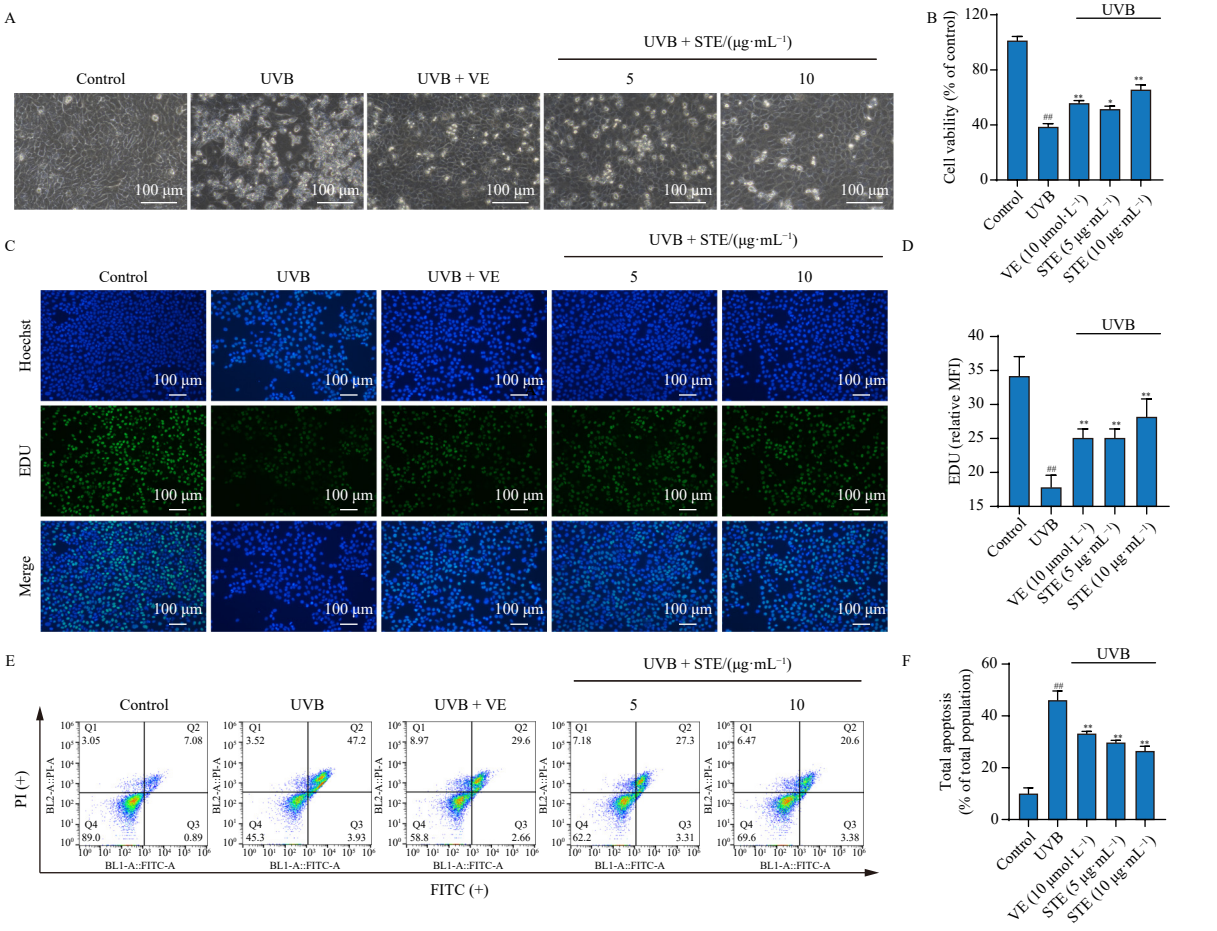

Fig. 1 STE protects HaCaT cells from UVB-induced reduction in cell viability and apoptosis.(A) Representative cell morphology in each group. Scale bar, 100 μm. (B) Cell proliferation in each group was assessed using the CCK-8 assay. (C) EdU proliferation assay in each group; EdU-positive cells are shown in green, and nuclei were stained with Hoechst 33342. Scale bar, 100 μm. (D) Percentage of EdU-positive proliferating cells in each group. (E) Apoptosis in each group was analyzed by flow cytometry. (F) Quantification of apoptotic cells in each group. Data are presented as mean ± SD (n = 3). Statistical comparisons were performed using one-way ANOVA analysis. $^{\#\#}P < 0.01$ *vs* the Control group; $^{*}P < 0.05$, $^{**}P < 0.01$ *vs* the UVB group.

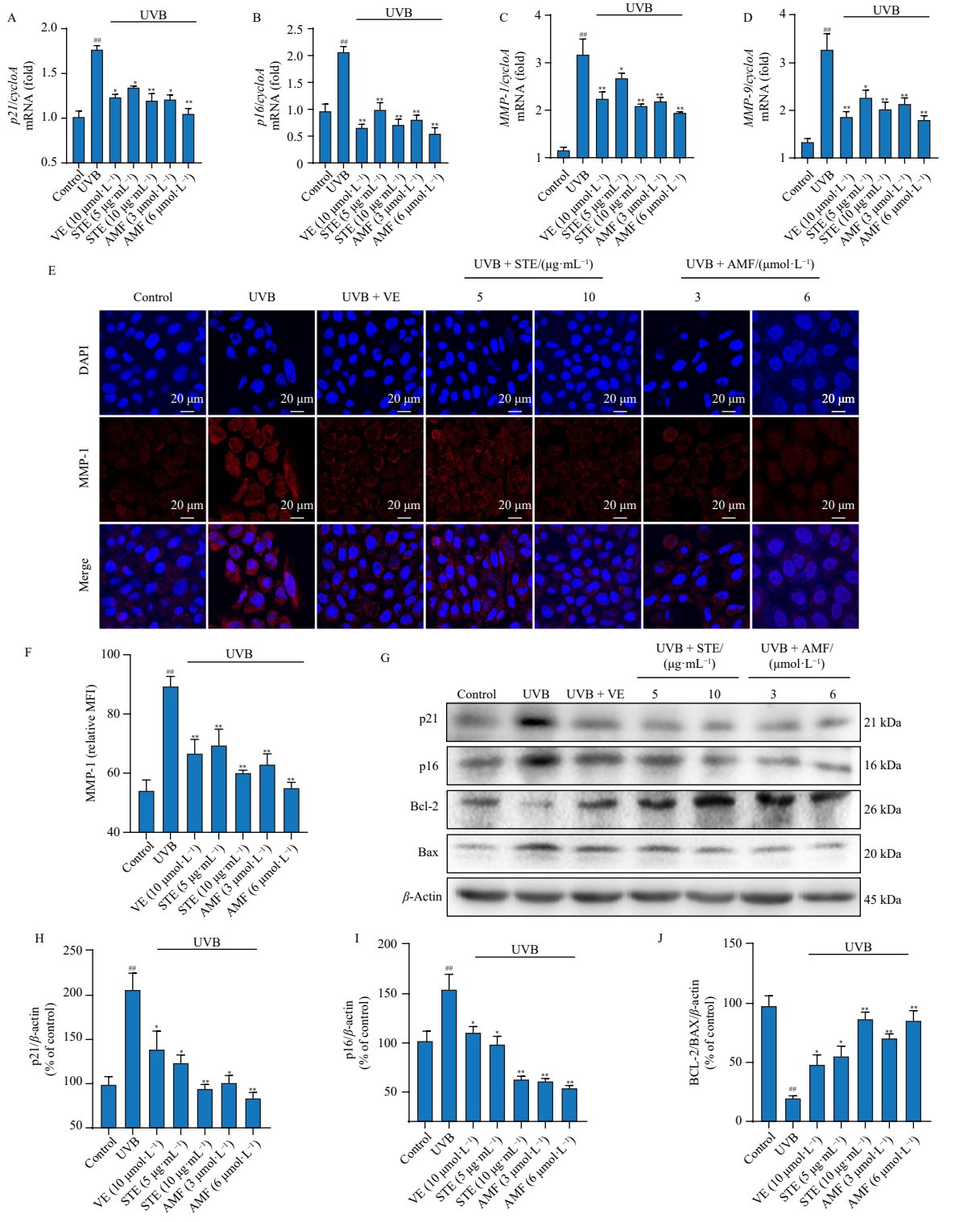

Fig. 2 STE and AMF protect HaCaT cells from UVB-induced cell aging. (A–D) Relative mRNA expression levels of *p21*, *p16*, *MMP-1*, and *MMP-9* in control and UVB-irradiated groups. (E, F) Representative images and quantification of MMP-1 in HaCaT cells by immunofluorescence. Scale bar, 20 μm. (G–J) Representative blots and quantitative analysis of p21, p16, Bcl-2, and Bax protein expression in HaCaT cells treated with STE or AMF. Data are presented as mean ± SD (n = 3). Statistical comparisons were performed using one-way ANOVA analysis. $^{\#\#}P < 0.01$ *vs* the Control group; $^{*}P < 0.05$, $^{**}P < 0.01$ *vs* the UVB group.

ure generates excessive reactive oxygen species (ROS), disrupts the antioxidant defense system, promotes lipid peroxidation, and reduces the activity of antioxidant enzymes such as superoxide dismutase (SOD) and catalase [27]. Our results showed that UVB exposure significantly reduced SOD activity and markedly increased MDA levels (Figs. 3A–3B),enhanced oxidative stress. STE and AMF effectively reversed these changes and alleviated UVB-induced oxidative stress. Inflammation is another hallmark event of photoaging process [28]. The mRNA expression levels of *IL-1β*, *TNF-α*, and *IL-6* were significantly increased after UVB exposure, whereas STE and AMF reversed these changes in a dose-dependent manner (Figs. 3C–3E). Immunofluorescence results further confirmed that both STE and AMF effectively mitigated the UVB-induced inflammatory response (Figs. 3F–3K). Notably, AMF at lower concentrations showed comparable or superior efficacy to STE, highlighting its role as a key active constituent. Collectively, these findings demonstrate the antioxidative and anti-inflammatory activities of STE and AMF in protecting keratinocytes from

UVB-induced damage.

3.5. STE and AMF alleviate UVB-induced photoaging in mouse skin

To further confirm the protective effects of STE and AMF against photoaging, a UVB-induced skin photoaging model was established in ICR mice (Fig. 4A). Visual observation of the dorsal skin showed that UVB exposure significantly increased skin roughness and caused epidermal damage. STE and AMF prevented these changes (Fig. 4B), effectively restored skin moisture (Fig. 4C), and alleviated UVB-induced oxidative stress (Figs. 4D and 4E). Histopathological analysis showed that the skin structure of the control group was intact, with a thin epidermis and tight dermal–epidermal connections. In contrast, the UVB-exposed group showed marked epidermal thickening, partial hyperkeratosis, and increased MMP-3 expression. Treatment with STE, AMF, or VE significantly reduced epidermal thickness and increased dermal collagen levels (Figs. 4F–4H). In addition, Western blot analysis showed that UVB exposure significantly in-

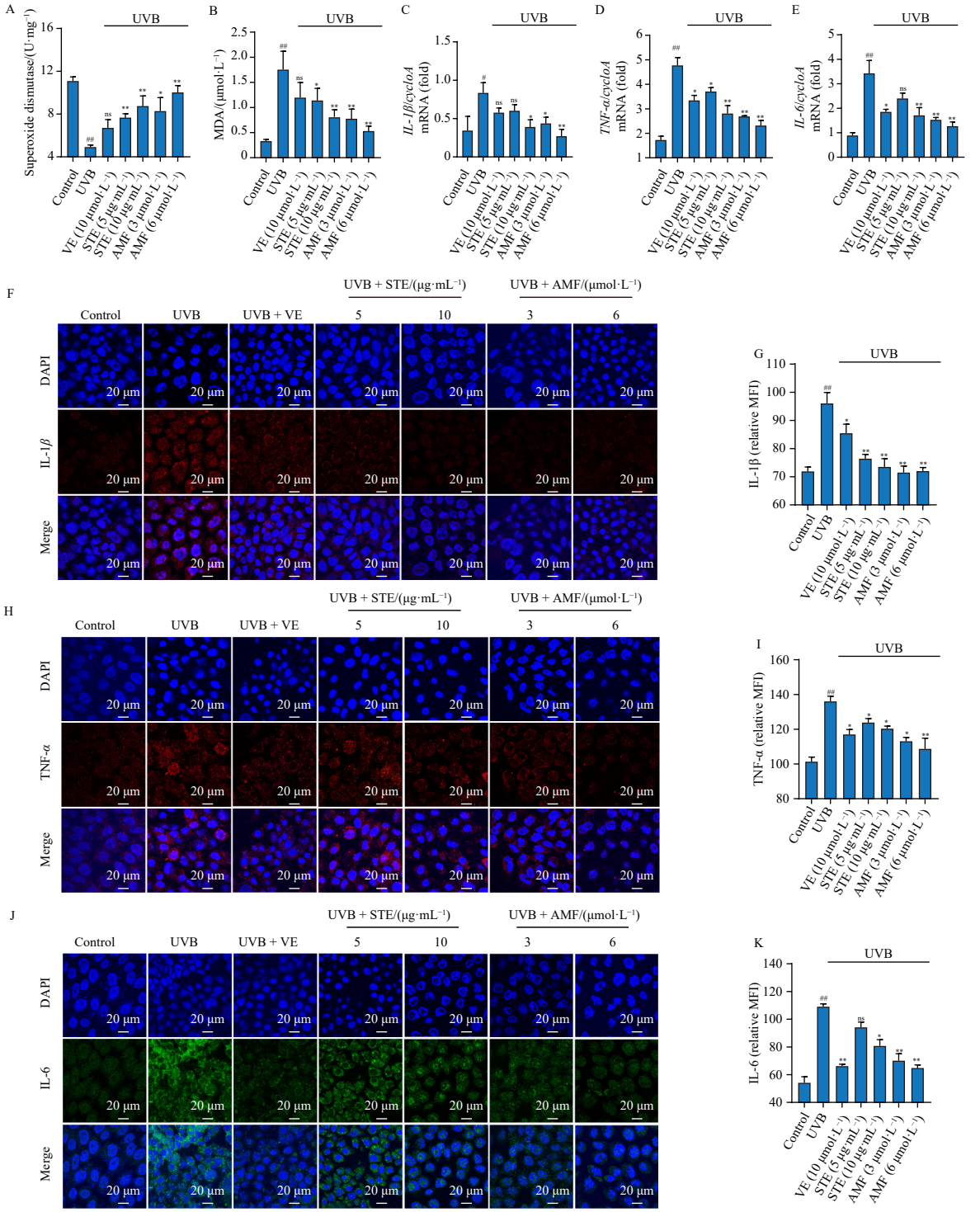

Fig. 3 STE and AMF alleviate UVB-induced oxidative stress and inflammation in cells. (A) SOD activity in HaCaT cells. (B) MDA levels in HaCaT cells. (C–E) Relative *IL-1β*, *TNF-α*, and *IL-6* mRNA expression in the control and UVB-irradiated groups. (F, G) Representative immunofluorescence images and quantification of IL-1β in HaCaT cells. Scale bar, 20 μm. (H, I) Representative immunofluorescence images and quantification of TNF-α in HaCaT cells. Scale bar, 20 μm. (J, K) Representative immunofluorescence images and quantification of IL-6 in HaCaT cells. Scale bar, 100 μm. Data are presented as mean ± SD (n = 3). Statistical comparisons were performed using one-way ANOVA analysis. $^{\#}P < 0.05$, $^{\#\#}P < 0.01$ *vs* the Control group; $^{*}P < 0.05$, $^{**}P < 0.01$ *vs* the UVB group; ns, no significant versus the UVB group.

creased the expression of MMP-1, p16, and p21 in mouse skin, whereas STE and AMF effectively reversed these changes (Figs. 4I–4L). Masson's trichrome staining showed that collagen fiber bundles were markedly decreased and sparsely distributed after UVB exposure. STE and AMF dose-dependently preserved dermal collagen integrity and prevented UVB-induced collagen degradation in mouse skin (Fig. 5A). Immunofluorescence analysis further showed a marked reduction in COL1A1 expression in the UVB-exposed group (Figs. 5B and 5C). Moreover, the expression of the inflammatory factors MMP-2 and IL-1β was markedly increased (Figs. 5D–5G), and STE and AMF treatment significantly reversed these changes. Consistent with the *in vitro* results, these results demonstrate that STE and AMF exert protective effects against photoaging in vivo.

3.6. Network pharmacology and GEO database analysis of AMF in the treatment of photoaging

Using a network pharmacology approach, 101 potential AMF targets were identified from multiple databases, alongside 312

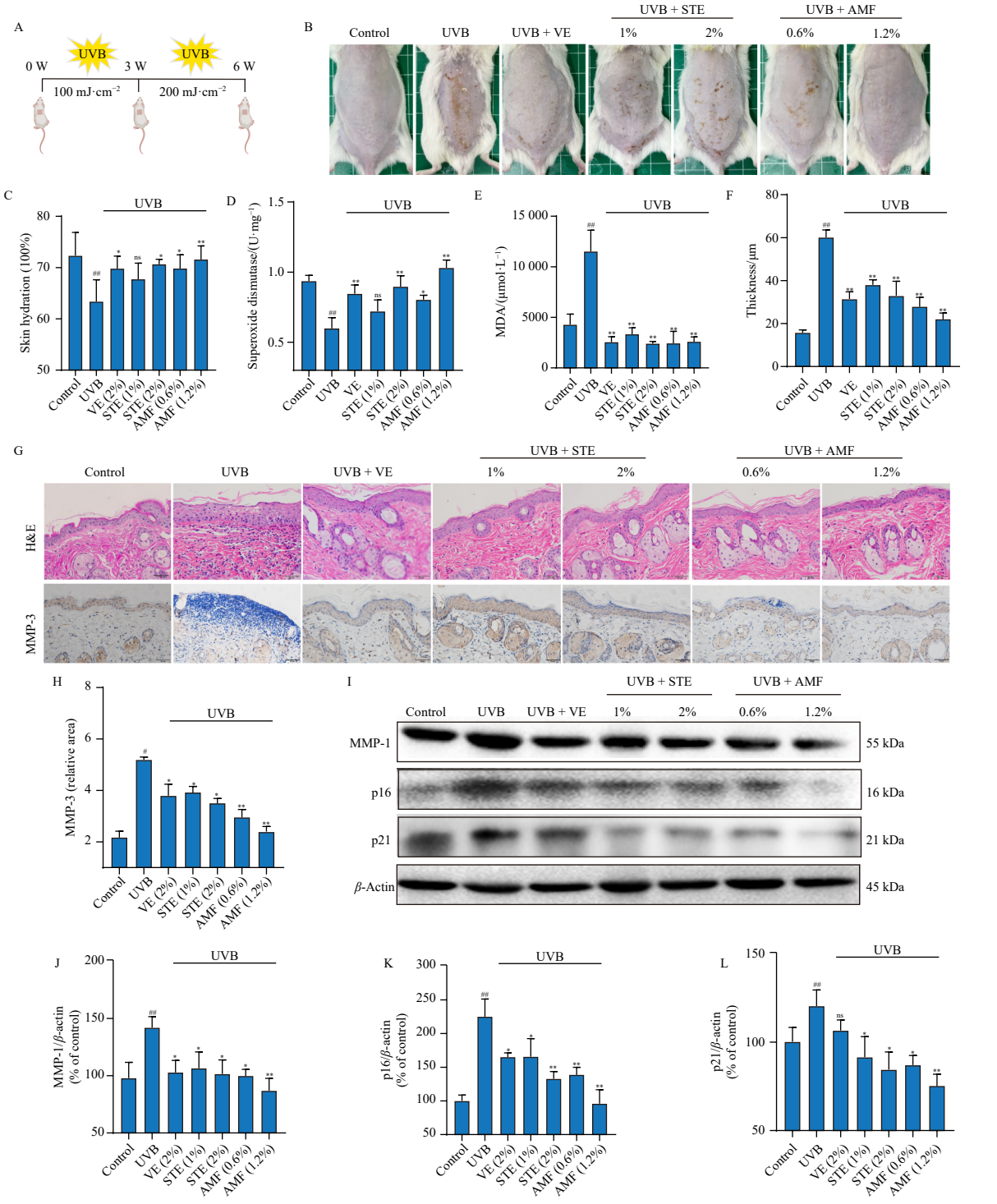

Fig. 4 STE and AMF alleviate UVB-induced skin photoaging damage *in vivo*. (A) Experimental methods *in vivo*. (B) Representative images of the mouse dorsal skin (n = 7). (C) Comparison of epidermal hydration in mice (n = 7). (D) SOD activity in the dorsal skin of mice (n = 7). (E) MDA levels in mouse dorsal skin (n = 5). (F) Epidermal thickness in mice (n = 7). (G) Representative images of H&E and MMP-3 in different groups. Scale bars, 50 and 100 μm. (H) Quantification of MMP-3 in different groups (n = 7). (I, J, K, L) Relative protein level of MMP-1, p16, and p21 in the control and UVB-radiation groups (n = 3). Data are presented as mean ± SD. Statistical comparisons were performed using one-way ANOVA analysis. $^{\#}P < 0.05$, $^{\#\#}P < 0.01$ *vs* the Control group; $^{*}P < 0.05$, $^{**}P < 0.01$ *vs* the UVB group; ns, no significant versus the UVB group.

key targets associated with photoaging. Intersection of these datasets yielded 20 common targets, including MMP-2, AKT1, and AMPK, as shown in the Venn diagram (Fig. 6A). These common targets were analyzed using the STRING database (https://cn.string-db.org/) to construct a protein–protein interaction (PPI) network and predict target interactions (Fig. 6B). Functional enrichment analysis was then performed to examine the biological relevance of these overlapping targets. GO and KEGG enrichment analyses showed that the intersecting targets were primarily involved in oxidative stress response, inflammatory regulation, and autophagy-related pathways (Figs. 6C and 6D).

AMPK, as a key energy sensor, is known to coordinate cellular defense mechanisms by enhancing antioxidant capacity, activating autophagy *via* ULK1 phosphorylation, and suppressing inflammation through inhibition of NF-κB signaling and NLRP3 inflammasome activation [29]. GEO dataset analysis confirmed that PRKAA1 expression was significantly downregulated in aged cells (Fig. 6E), alongside reduced expression of autophagy-related genes (ULK1, BECN1, MAP1LC3A) and increased SQSTM1 (p62) accumulation (Figs. 6F–6I). These findings suggest that AMF may mitigate photoaging by restoring AMPK activity, thereby enhancing redox homeostasis, promoting autophagy, and attenuating inflammation.

3.7. AMPK is a key target of AMF

To investigate the potential targets and molecular mechanisms of AMF, molecular docking was performed between AMF and AMPK. The results demonstrated that the dimeric structure of AMF fit well within the binding cavity of AMPK. AMF formed hydrogen bonds with selenocysteine residues in AMPK and ionic interactions with arginine residues (Figs. 7A and 7B). CETSA is commonly used to examine the interaction between donors and receptors [30]. As temperature increased, protein denaturation also increased; however, the addition of AMF significantly enhanced

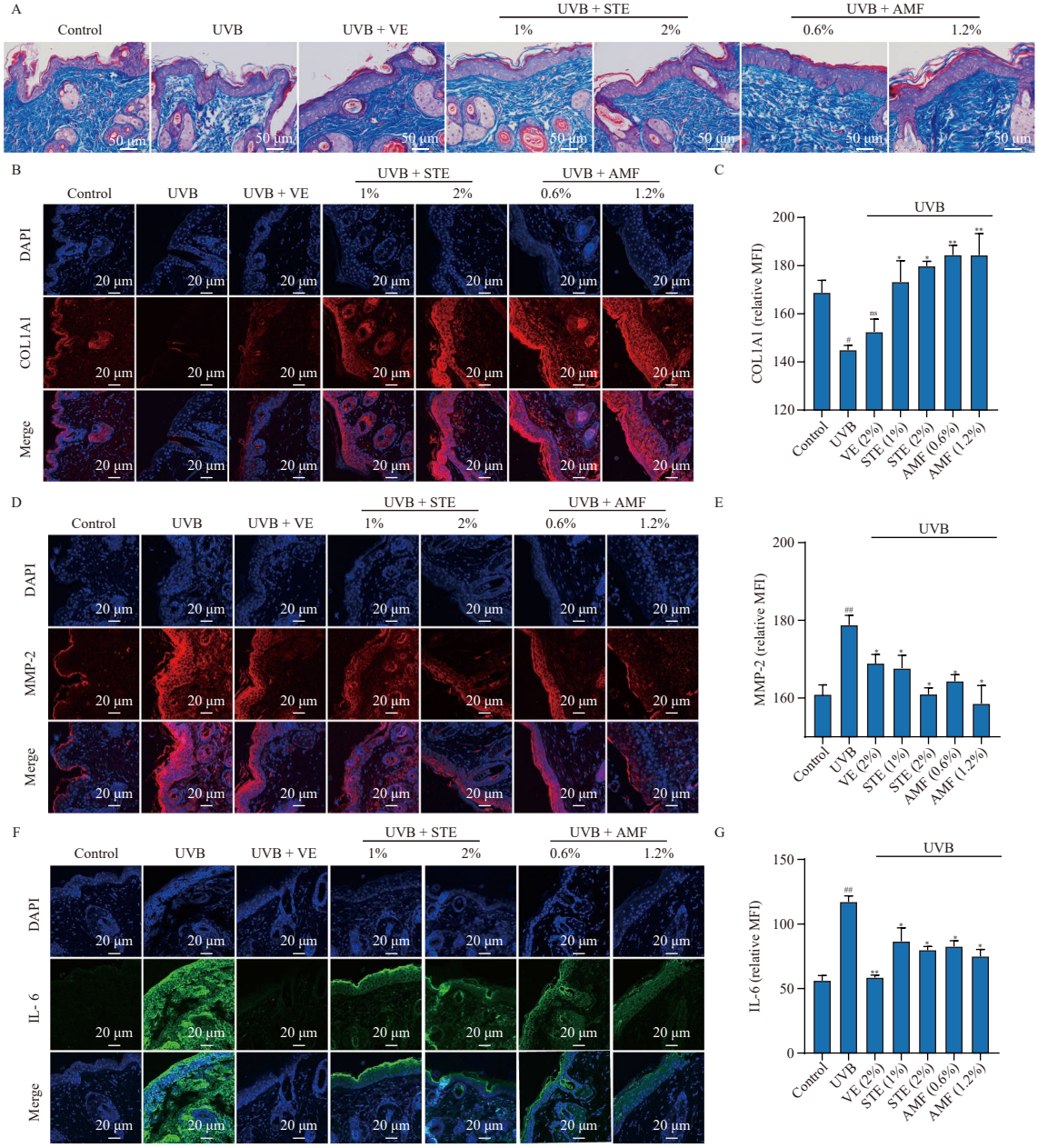

Fig. 5 STE and AMF restore collagen balance and inflammatory response in mouse skin. (A) Masson staining of mouse dorsal skin. Scale bar, 100 μm. (B, C) Immunofluorescence images and quantification of COL1A1 in mouse dorsal skin. Scale bar, 100 μm. (D, E) Immunofluorescence images and quantification of MMP-2 in mouse dorsal skin. Scale bar, 100 μm. (F, G) Immunofluorescence images and quantification of IL-6 in mouse dorsal skin. Scale bar, 20 μm. Data are presented as mean ± SD (n = 7). Statistical comparisons were performed using one-way ANOVA analysis. $^{\#}P < 0.05$, $^{\#\#}P < 0.01$ *vs* the Control group; $^{*}P < 0.05$, $^{**}P < 0.01$ *vs* the UVB group; ns, no significant versus the UVB group.

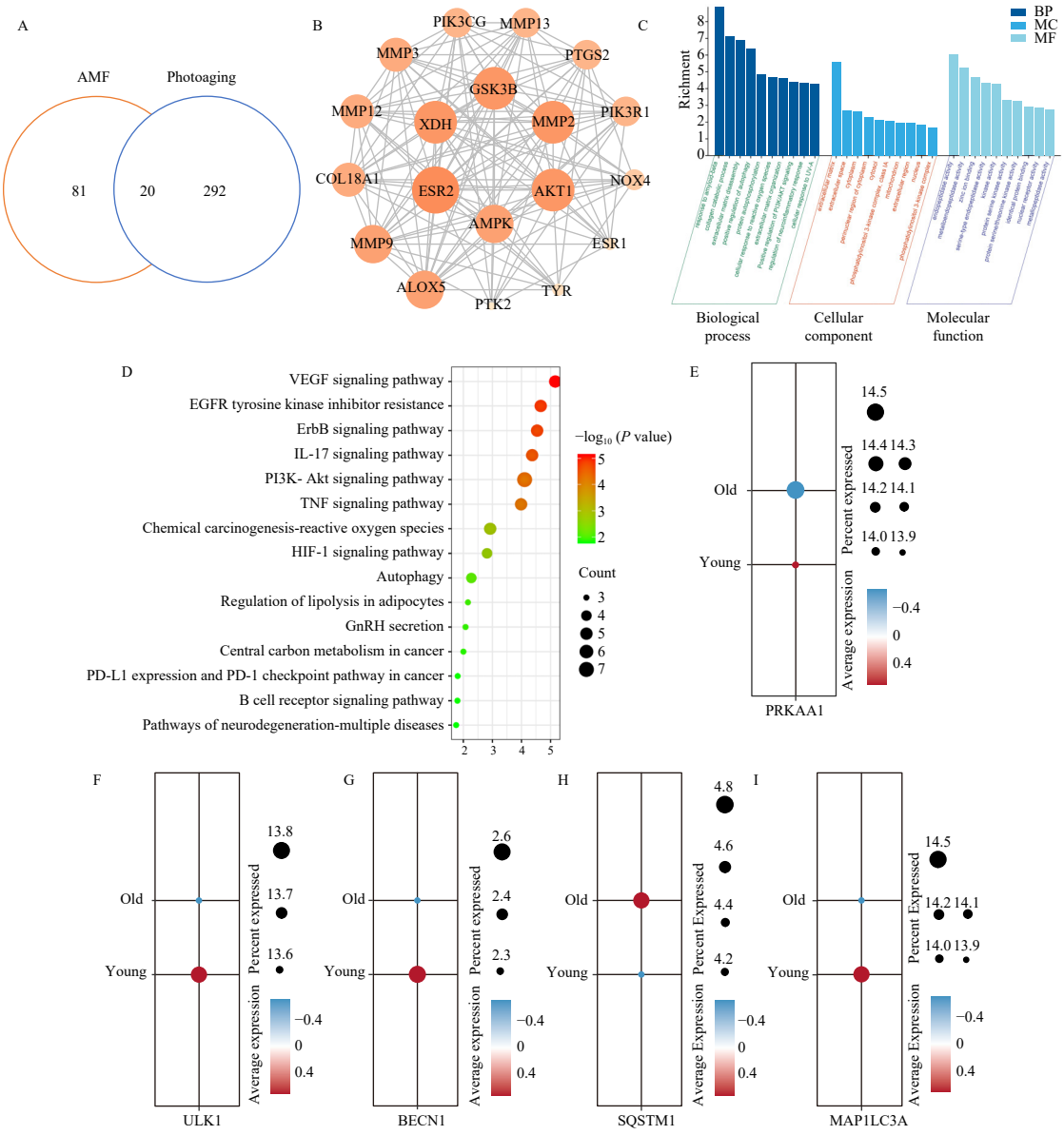

Fig. 6 Network pharmacology analysis of AMF in the treatment of photoaging. (A) Venn diagram of potential targets of AMF against photoaging. (B) PPI network of the common targets of AMF against photoaging. (C) Results of GO enrichment analysis. (D) Results of KEGG enrichment analysis. (E–I) Dot plots showing the overall expression levels of *PRKAA1, ULK1, BECN1, SQSTM1, and MAP1LC3A* across age groups.

the thermal stability of AMPK, particularly at 53 °C, compared with the DMSO control. Further ITDRF$_{CETSA}$ analysis revealed that AMPK thermal stability increased in a dose-dependent manner in the presence of AMF (Figs. 7C–7F). These findings suggest that AMF can directly bind to AMPK to exert its activating effect. In addition, after HaCaT cells were co-cultured at the specified dose (3, 6 μmol·L^{-1}), AMF significantly increased AMPK phosphorylation, activated the downstream protein ULK1, increased the LC3-II/LC3-I ratio and Beclin-1 expression, and reduced p62 expression in a dose-dependent manner. AMF did not affect mTOR phosphorylation (Figs. 7G–7M). Collectively, these results indicate that AMF activates AMPK and engages ULK1-dependent autophagy pathways.

3.8. AMF alleviates photoaging by activating the AMPK/ULK1 pathway

In our study, inhibition of AMPK with CC eliminated AMF-mediated cytoprotection against UVB, as evidenced by abnormal morphology, decreased viability, and suppressed proliferation (Figs. 8A–8D). These findings demonstrate that AMF exerts its anti-photoaging effects *via* AMPK activation. Accordingly, we examined downstream AMPK signaling to delineate the mechanism. Autophagy is one of the key pathways involved in aging [31]. AMPK can directly interact with the autophagy-related protein ULK1, thereby activating the entire autophagy pathway [32]. Transmission electron microscopy and the tandem mRFP-GFP-LC3 reporter demonstrated increased autophagic flux with AMF compared with UVB-treated cells (Figs. 8E–8H). AMF effectively reversed these changes, promoted the conversion of LC3-I to LC3-II, and facilitated autophagosome formation, thereby suppressing the expression of p16, p21, and MMP-1. However, the addition of CC reversed the autophagy-promoting and anti-photoaging effects of AMF (Fig. 8I, Supplementary Fig. S13). In addition, UVB irradiation markedly increased *IL-1β*, *TNF-α*, and *IL-6* mRNA. Pretreatment with AMF significantly attenuated these inductions. However, this effect was abolished by AMPK inhibition with CC or by inhibition of early autophagy with 3-MA, indicating that the anti-inflammatory effect of AMF is AMPK-dependent and requires intact early autophagy (Figs. 8J–8L). Metformin was used as the AMPK activator because it activates AMPK upstream and induces autophagy [33, 34], providing a mechanism-aligned and

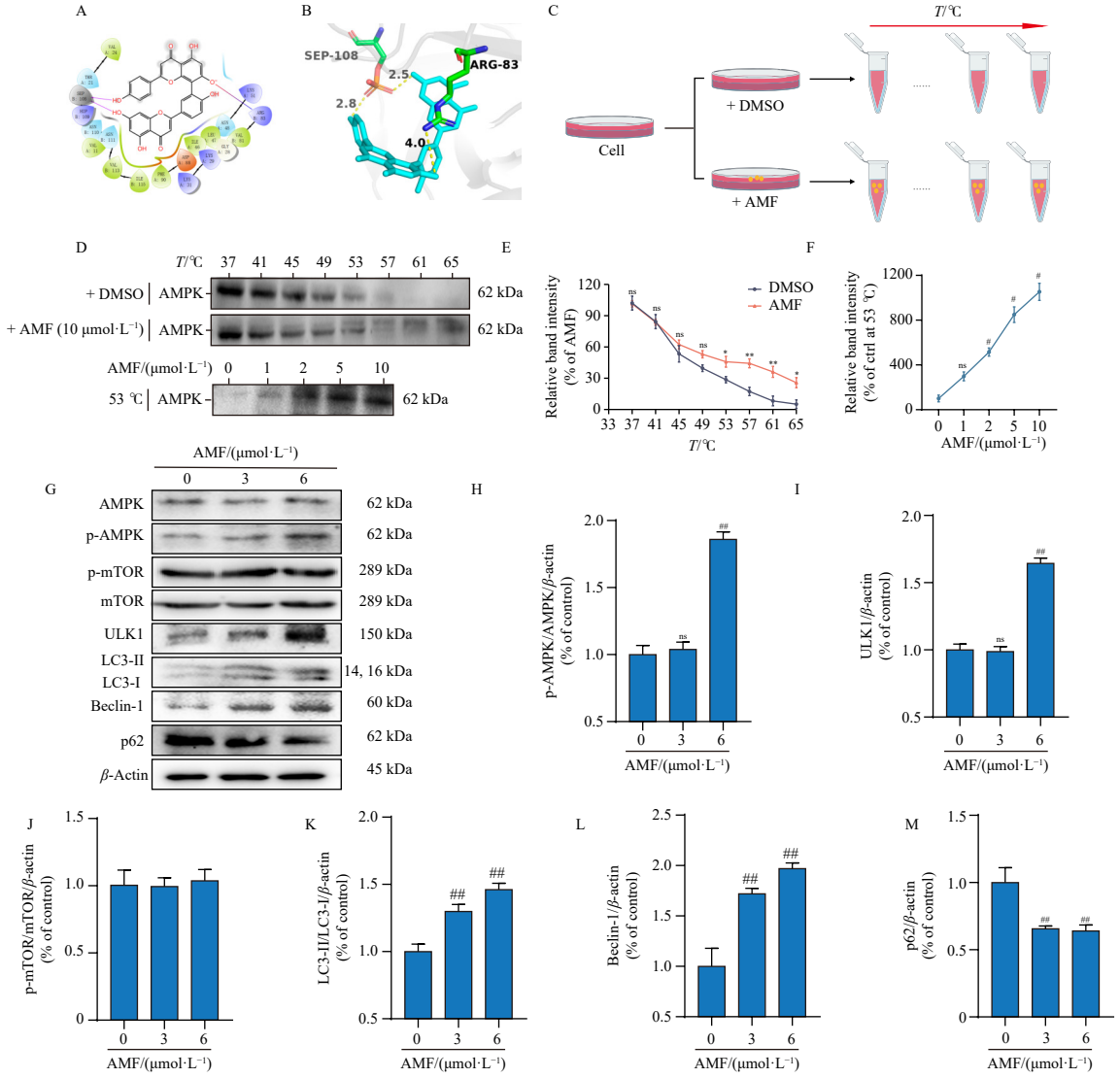

Fig. 7 AMPK is a key target of AMF. (A, B) Molecular docking of AMF with AMPK. (C–F) Flowchart and results of CETSA and ITDRF$_{CETSA}$ assay. (G–M) Representative blots and quantitation of AMPK, p-AMPK, mTOR, p-mTOR, ULK1, LC3 Ⅱ / Ⅰ, Beclin-1, and p62 proteins in HaCaT cells treated by AMF . Data are presented as mean ± SD (n = 3). Statistical comparisons were performed using one-way ANOVA analysis. $^{\#}P < 0.05$, $^{\#\#}P < 0.01$ *vs* the Control group; $^{*}P < 0.05$, $^{**}P < 0.01$ *vs* the DMSO treatment group; ns, no significant versus the DMSO treatment group or the UVB group.

translationally relevant benchmark for AMF. In our study, MET increased autophagy and reduced senescence. AMF did not alter total mTOR or p-mTOR levels. Furthermore, AMPK knockdown reduced Beclin-1 expression and LC3 conversion, prevented AMF-induced ULK1 activation, and abolished both the autophagic and anti-photoaging effects of AMF, as well as its anti-inflammatory effects (Figs. 8M–8P, Supplementary Fig. S14). These findings support a model in which AMF mitigates photoaging primarily by activating AMPK and engaging the ULK1-dependent autophagy pathway (Fig. 9).

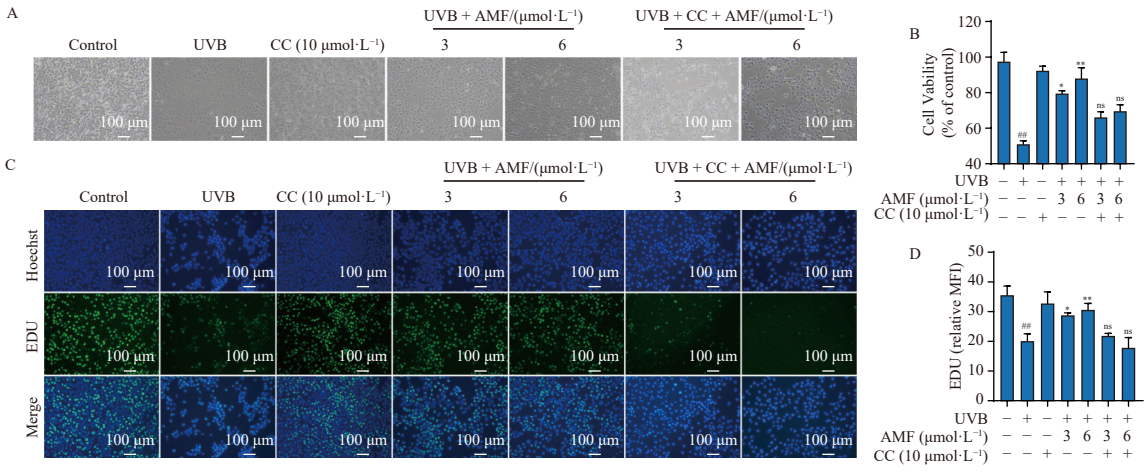

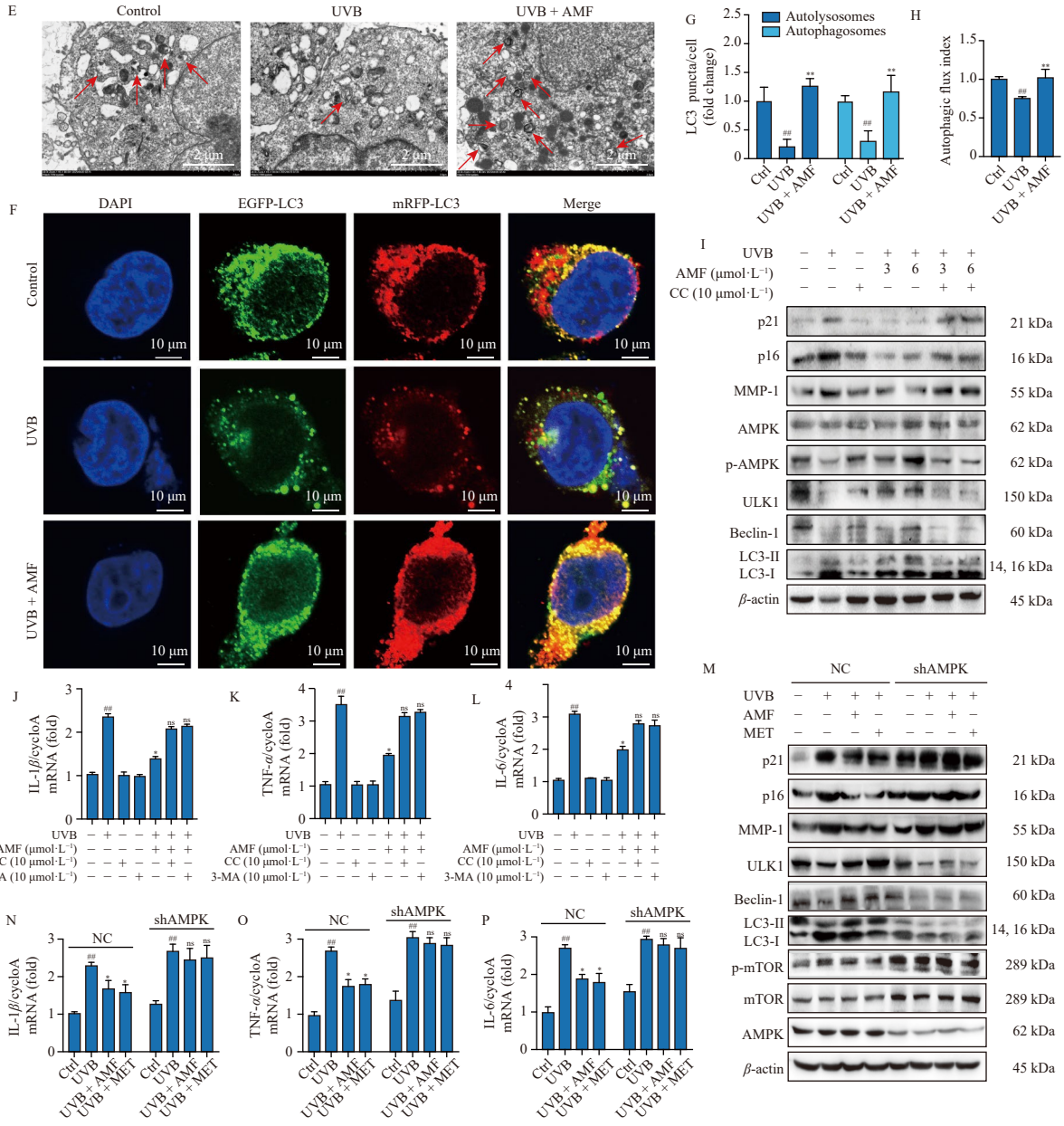

Fig. 8 AMF alleviates photoaging by activating the AMPK/ULK1 pathway. (A) Representative images of cell morphology. Scale bar, 100 μm. (B) Cell proliferation in each group was assessed using the CCK-8 assay. (C, D) Transmission electron microscopy of HaCaT cells under control conditions, UVB exposure, or AMF treatment. Arrows indicate autophagosomes. Scale bar, 2 μm. (F–H) Representative confocal images and quantification of mRFP-GFP-LC3 puncta and the autophagic flux index in HaCaT cells after lentiviral transduction. Red dots indicate autolysosomes, and yellow dots indicate autophagosomes. The autophagic flux index, R/(R + Y), was calculated as the proportion of red-only puncta among the total red-only plus yellow puncta. An increase in R/(R + Y) indicates enhanced autophagic degradation. Scale bar, 10 μm. (I) Representative Western blots of p21, p16, MMP-1, AMPK, p-AMPK, ULK1, Beclin-1, and LC3-II/I in HaCaT cells treated with UVB, AMF, and CC. (J–L) Relative *IL-1β*, *TNF-α*, and *IL-6* mRNA expression in the HaCaT cells treated with UVB, AMF, CC or 3-MA. (M) Representative Western blots of p21, p16, MMP-1, AMPK, ULK1, mTOR, Beclin-1, and the LC3-II/I ratio in HaCaT cells transfected with shAMPK. (N–P) Relative *IL-1β*, *TNF-α*, and *IL-6* mRNA expression in the HaCaT cells transfected with shAMPK. Data are presented as mean ± SD (n = 3). Statistical comparisons were performed using one-way ANOVA or two-way ANOVA analysis. $^{\#\#}P < 0.01$ *vs* the Control group; $^{*}P < 0.05$, $^{**}P < 0.01$ *vs* the UVB group; ns, no significant versus the UVB group.

3.9. Skin toxicity, permeability, and stability of STE and AMF

The skin toxicity, permeability, and stability of STE and AMF were systematically evaluated to assess the clinical applicability. Acute skin toxicity tests revealed no abnormal reactions in mice treated with STE or AMF. Body weights were comparable to those of controls in both intact and damaged skin mice (Fig. S15A). No erythema, mortality, or significant morphological changes were observed, indicating that topical STE and AMF were well tolerated and showed no apparent toxicity (Figs. S15B–S15D). *In vitro* skin permeation studies were performed to assess the transdermal delivery of AMF emulsion. AMF emulsion reached a plateau at 12 h, and the cumulative permeation reached 17.95 ± 3.43 μg·cm^{-2} at 24 h (Fig. S16). Stability testing under high temperature, high humidity, and intense light exposure showed no obvious changes in appearance; AMF remained a yellow, odorless powder throughout the study. Its content consistently remained within the acceptable range (95.0%–105.0%) (Table S3). These findings indicate that AMF has good stability under the tested stress conditions.

4. Discussion

UVB radiation, a major component of mid-wave ultraviolet light, exerts highly destructive effects on skin cells and is a primary contributor to skin photoaging [35]. penetrates the epidermis to reach the basal layer, causing molecular damage and activating pathways associated with oxidative stress and inflam-

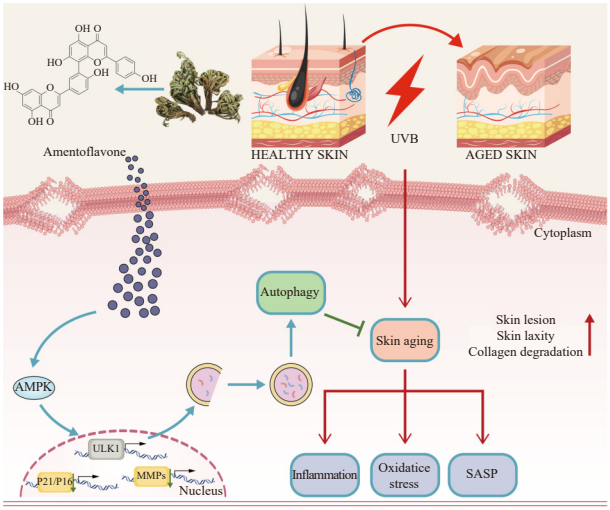

Fig. 9 Schematic diagram of the anti-photoaging mechanism of AMF. AMF activates AMPK and engages ULK1-dependent autophagy, thereby alleviating UVB-induced skin inflammation and collagen degradation and ultimately mitigating photoaging.

mation [36]. UVB exposure induces high levels of ROS [37], which impair the natural antioxidant defense system of skin [38] by reducing the activity and expression of key detoxifying enzymes such as catalase and superoxide dismutase. Accumulated ROS interact with cellular lipids, leading to lipid peroxidation and the formation of cytotoxic products such as MDA. At the same time, ROS activate inflammation-related pathways, including NF-κB [39, 40], which upregulates the expression of pro-inflammatory cytokines such as IL-6, IL-1β, and TNF-α. These processes collectively contribute to structural damage and accelerate photoaging.

S. tamariscina, a traditional Chinese medicine abundant in flavonoids, has demonstrated significant antioxidant and anti-inflammatory properties [16], making it a promising candidate for the prevention of skin photoaging. AMF is the primary active component of STE. In this study, UVB exposure reduced SOD activity, increased MDA levels, and elevated inflammatory cytokines in HaCaT cells and mouse epidermal tissue. STE and AMF significantly reversed these changes, alleviating oxidative stress and inflammation. Additionally, UVB exposure suppresses cell proliferation and induces apoptosis [41], accompanied by an upregulation of cell cycle regulators p21 and p16, which contribute to G_1 phase arrest and irreversible cellular senescence [42]. STE and AMF effectively inhibited UVB-induced senescence and apoptosis in a dose-dependent manner by reducing p21 and p16 expression. These findings indicate that STE and AMF protect against UVB-induced photoaging by attenuating oxidative damage, inflammation, and cellular senescence. Consistent with component analysis and activity evaluation, AMF appears to be the principal contributor to STE activity. However, given the multi-component nature of STE, potential contributions from minor constituents cannot be completely excluded and warrant further investigation.

Collagen, the most abundant structural protein in the skin, is essential for maintaining structural integrity, elasticity, and repair capacity. Its metabolism is largely regulated by MMPs [26], particularly collagenase-1 (MMP-1), gelatinase-A (MMP-2), and stromelysin-1 (MMP-3), which degrade type I, III, and IV collagen. These enzymes are critical for extracellular matrix remodeling under physiological conditions [43]. However, UVB exposure markedly upregulates MMP expression, leading to excessive collagen degradation and disruption of matrix homeostasis, ultimately resulting in skin thinning, reduced elasticity, and moisture loss [44]. n this study, STE and AMF effectively suppressed UVB-induced expression of MMP-1, MMP-2, and MMP-3, while enhancing COL1A1 expression, thereby reducing epidermal thickening and moisture loss.

To further investigate the mechanism of AMF, network pharmacology analysis suggested a key role for autophagy. Autophagy is a protective cellular process that maintains homeostasis by degrading and recycling damaged proteins and organelles under stress conditions [45, 46]. ULK1, the initiating kinase of autophagy, plays a critical role in promoting autophagosome formation, Beclin-1 complex assembly, autophagosome elongation, and autophagic membrane expansion upon activation. Additionally, ULK1 facilitates LC3 lipidation, converting LC3-I to LC3-II, which enables autophagosomes to efficiently sequester and degrade damaged cellular components. ULK1 activation also regulates selective autophagy receptors, such as p62, which assist in recognizing and transporting abnormal substances, thus conferring selectivity to the autophagic process [47, 48]. UVB exposure disrupts cellular homeostasis, leading cells to spontaneously activate autophagy as a defense mechanism. However, excessive UVB exposure can inhibit autophagic processes [49]. In this study, UVB reduced ULK1 and Beclin-1 expression, increased p62 levels, and disrupted LC3 conversion, indicating impaired autophagy. AMF treatment reversed these alterations, suggesting that it mitigates photoaging by restoring autophagic activity.

Autophagy, a key process in longevity regulation, is intimately linked to changes in energy metabolism. Increasing evidence suggests that AMPK signaling is a major regulator of autophagy [10]. It can directly phosphorylate and activate the autophagy-initiating complex ULK1, thereby initiating the autophagic pathway [50]. In this study, network pharmacology analysis identified AMPK as a potential primary target of AMF. Molecular docking analysis revealed that AMF fits well within the AMPK subunit cavity, forming multiple hydrogen bonds with the protein. CETSA experiments further confirmed the direct binding of AMF to AMPK. Moreover, the addition of the AMPK inhibitor Compound C or shAMPK transfection significantly reduced the anti-photoaging activity of AMF and suppressed autophagy, indicating that AMF exerts its anti-photoaging effects through AMPK activation. Studies have shown that AMPK positively regulates autophagy by activating ULK1 and restraining mTOR [51]. In our study, AMF activated AMPK and engaged the ULK1 pathway, promoting autophagy and mitigating UVB-induced photoaging. AMF did not measurably alter mTOR phosphorylation, possibly reflecting only a modest effect on mTOR. Overall, these findings indicate that AMF primarily activates AMPK and preferentially engages ULK1-dependent autophagy in this model.

As a central energy sensor, AMPK regulates multiple signaling pathways, including NF-κB pathway [29]. In UVB-exposed HaCaT cells, AMF suppressed the induction of IL-6, IL-1β, and TNF-α, consistent with attenuation of NF-κB activity. Increasing evidence indicates that autophagy can limit inflammatory responses by removing inflammasome components [52]. Although 3-MA is widely used as an autophagy inhibitor, it can also inhibit class I PI3K [53], thereby altering inflammatory cytokine production independently of autophagy. In our study, 3-MA significantly blunted the ability of AMF to reduce UVB-induced IL-1β, IL-6, and TNF-α expression. Therefore, these findings were interpreted together with autophagic flux analysis, LC3/p62 and ULK1/Beclin-1 signaling, and AMPK knockdown results, which collectively support that AMF exerts anti-inflammatory effects primarily through AMPK-mediated autophagy.

This study provides a preliminary evaluation of the druggability of AMF. The results indicate that AMF exhibits good dermal tolerability, supports transdermal delivery, and maintains stability under stress conditions. However, further studies are required to optimize formulation, enhance dermal bioavailability, and evaluate long-term safety. In particular, optimizing delivery systems to improve skin retention and permeability while minimizing systemic exposure, together with systematic release and

permeation studies, will facilitate clinical translation.

5. Conclusion

This study demonstrates that STE and AMF, the primary active substance of *S. tamariscina*, exhibit potent anti-photoaging effects by effectively mitigating UVB-induced oxidative stress and inflammation, downregulating MMPs expression, and preventing collagen degradation. Mechanistically, AMF acts as a potential AMPK activator and promotes autophagy through the AMPK/ULK1 pathway, thereby contributing to its anti-photoaging activity. Druggability assessment further indicates that STE and AMF exhibit good stability and no detectable skin toxicity. These findings provide evidence supporting the therapeutic potential of STE and AMF in the treatment of photoaging and clarify the underlying mechanism of AMF, suggesting their promise as candidate agents for skin photoaging intervention.

Funding

This study was supported by the National Natural Science Foundation of China (Nos. 82273817, and 81973206), the China Postdoctoral Science Foundation (No. 2024M763662).

Ethics approval and consent to participate

The animal study protocol was approved by the Institutional Animal Care and Use Committee at China Pharmaceutical University (No. SYXK2021-0011).

Declaration of competing interest

No potential competing interests were reported by the authors.

References

1 Blume-Peytavi U, Kottner J, Sterry W, et al. Age-associated skin conditions and diseases: current perspectives and future options. *Gerontologist*. 2016;56(Suppl 2):S230-242. https://doi.org/10.1093/geront/gnw003.
2 Gu YP, Han JX, Jiang CP, et al. Biomarkers, oxidative stress and autophagy in skin aging. *Ageing Res Rev*. 2020;59:101036. https://doi.org/10.1016/j.arr.2020.101036.
3 Han AN, Chien AL, Kang S. Photoaging. *Dermatol Clin*. 2014;32:291-299, vii. https://doi.org/10.1016/j.det.2014.03.015.
4 Kammeyer A, Luiten RM. Oxidation events and skin aging. *Ageing Res Rev*. 2015;21:16-29. https://doi.org/10.1016/j.arr.2015.01.001.
5 Kim CW, Alam MB, Song BR, et al. γ-Mangosteen, an autophagy enhancer, prevents skin-aging *via* activating KEAP1/NRF2 signaling and downregulating MAPKs/AP-1/NF-κB-mediated MMPs. *Phytomedicine*. 2024;132:155815. https://doi.org/10.1016/j.phymed.2024.155815.
6 Wang SQ, Balagula Y, Osterwalder U. Photoprotection: a review of the current and future technologies. *Dermatol Ther*. 2010;23:31-47. https://doi.org/10.1111/j.1529-8019.2009.01289.x.
7 Rittié L, Fisher GJ. UV-light-induced signal cascades and skin aging. *Ageing Res Rev*. 2002;1:705-720. https://doi.org/10.1016/s1568-1637(02)00024-7.
8 Salminen A, Kaarniranta K. AMP-activated protein kinase (AMPK) controls the aging process *via* an integrated signaling network. *Ageing Res Rev*. 2012;11:230-241. https://doi.org/10.1016/j.arr.2011.12.005.
9 Apfeld J, O'connor G, Mcdonagh T, et al. The AMP-activated protein kinase AAK-2 links energy levels and insulin-like signals to lifespan in *C. elegans*. *Genes Dev*. 2004;18:3004-3009. https://doi.org/10.1101/gad.1255404.
10 Burkewitz K, Zhang Y, Mair WB. AMPK at the nexus of energetics and aging. *Cell Metab*. 2014;20:10-25. https://doi.org/10.1016/j.cmet.2014.03.002.
11 Meléndez A, Tallóczy Z, Seaman M, et al. Autophagy genes are essential for dauer development and life-span extension in *C. elegans*. *Science*. 2003;301:1387-1391. https://doi.org/10.1126/science.1087782.
12 Rubinsztein DC, Mariño G, Kroemer G. Autophagy and aging. *Cell*. 2011;146:682-695. https://doi.org/10.1016/j.cell.2011.07.030.
13 Wang M, Charareh P, Lei X, et al. Autophagy: multiple mechanisms to protect skin from ultraviolet radiation-driven photoaging. *Oxid Med Cell Longev*. 2019;2019:8135985. https://doi.org/10.1155/2019/8135985.
14 Zhao YL, Lin JJ, Li JN, et al. RhFGF21 protects epidermal cells against UVB-induced apoptosis through activating AMPK-mediated autophagy. *Int J Mol Sci*. 2022;23:12466. https://doi.org/10.3390/ijms232012466.
15 Xu ZT, Fu X, Jin LJ. Chemical constituents research progress of *Selaginella tamariscina*. *Chin J Mod Appl Pharm*. 2017;34:1779-1784. https://doi.org/10.13748/j.cnki.issn1007-7693.2017.12.030.
16 Bailly C. The traditional and modern uses of *Selaginella tamariscina* (*P. Beauv.*) Spring, in medicine and cosmetic: applications and bioactive ingredients. *J Ethnopharmacol*. 2021;280:114444. https://doi.org/10.1016/j.jep.2021.114444.
17 Lee H, Kim SY, Lee SW, et al. Amentoflavone-enriched *Selaginella rossii* protects against ultraviolet- and oxidative stress-induced aging in skin cells. *Life (Basel)*. 2022;12:2106. https://doi.org/10.3390/life12122106.
18 Yang JW, Pokharel YR, Kim MR, et al. Inhibition of inducible nitric oxide synthase by sumaflavone isolated from *Selaginella tamariscina*. *J Ethnopharmacol*. 2006;105:107-113. https://doi.org/10.1016/j.jep.2005.10.001.
19 Lee CW, Choi HJ, Kim HS, et al. Biflavonoids isolated from *Selaginella tamariscina* regulate the expression of matrix metalloproteinase in human skin fibroblasts. *Bioorg Med Chem*. 2008;16:732-738. https://doi.org/10.1016/j.bmc.2007.10.036.
20 De Almeida LGN, Thode H, Eslambolchi Y, et al. Matrix metalloproteinases: from molecular mechanisms to physiology, pathophysiology, and pharmacology. *Pharmacol Rev*. 2022;74:712-768. https://doi.org/10.1124/pharmrev.121.000349.
21 Park NH, Lee CW, Bae JH, et al. Protective effects of amentoflavone on Lamin A-dependent UVB-induced nuclear aberration in normal human fibroblasts. *Bioorg Med Chem Lett*. 2011;21:6482-6484. https://doi.org/10.1016/j.bmcl.2011.08.067.
22 Liu KS, Huang TH, Aljuffali IA, et al. Exploring the structure-permeation relationship of topical tricyclic antidepressants used for skin analgesia. *Int J Pharm*. 2017;523:386-397. https://doi.org/10.1016/j.ijpharm.2017.03.048.
23 *Pharmacopoeia of the People's Republic of China*. Beijing: China Medical Science and Technology Press. 2020.
24 Bhatia-Dey N, Kanherkar RR, Stair SE, et al. Cellular senescence as the causal nexus of aging. *Front Genet*. 2016;7:13. https://doi.org/10.3389/fgene.2016.00013.
25 Zhang WW, Zheng ZT, Wang TY, et al. Succinylated type I collagen regulates ferroptosis to attenuate skin photoaging. *ACS Appl Mater Interfaces*. 2024;16:56744-56761. https://doi.org/10.1021/acsami.4c11952.
26 Jabłońska-Trypuć A, Matejczyk M, Rosochacki S. Matrix metalloproteinases (MMPs), the main extracellular matrix (ECM) enzymes in collagen degradation, as a target for anticancer drugs. *J Enzyme Inhib Med Chem*. 2016;31:177-183. https://doi.org/10.3109/14756366.2016.1161620.
27 He L, He T, Farrar S, et al. Antioxidants maintain cellular redox homeostasis by elimination of reactive oxygen species. *Cell Physiol Biochem*. 2017;44:532-553. https://doi.org/10.1159/000485089.
28 Wang YJ, Wang L, Wen X, et al. NF-κB signaling in skin aging. *Mech Ageing Dev*. 2019;184:111160. https://doi.org/10.1016/j.mad.2019.111160.
29 Garcia D, Shaw RJ. AMPK: mechanisms of cellular energy sensing and restoration of metabolic balance. *Mol Cell*. 2017;66:789-800. https://doi.org/10.1016/j.molcel.2017.05.032.
30 Gao CL, Hou GG, Liu J, et al. Synthesis and target identification of benzoxepane derivatives as potential anti-neuroinflammatory agents for ischemic stroke. *Angew Chem Int Ed Engl*. 2020;59:2429-2439. https://doi.org/10.1002/anie.201912489.
31 Kaushik S, Tasset I, Arias E, et al. Autophagy and the hallmarks of aging. *Ageing Res Rev*. 2021;72:101468. https://doi.org/10.1016/j.arr.2021.101468.
32 Park JM, Lee DH, Kim DH. Redefining the role of AMPK in autophagy and the energy stress response. *Nat Commun*. 2023;14:2994. https://doi.org/10.1038/s41467-023-38401-z.
33 Yang F, Qin Y, Wang YQ, et al. Metformin inhibits the NLRP3 inflammasome *via* AMPK/mTOR-dependent effects in diabetic cardiomyopathy. *Int J Biol Sci*. 2019;15:1010-1019. https://doi.org/10.7150/ijbs.29680.
34 Zhu JP, Zhang ZZ, Yang QY, et al. Metformin attenuates sevoflurane-induced neurocognitive impairment through AMPK-ULK1-dependent autophagy in aged mice. *Brain Res Bull*. 2020;157:18-25. https://doi.org/10.1016/j.brainresbull.2020.01.018.
35 Tang XY, Yang TY, Yu DJ, et al. Current insights and future perspectives of ultraviolet radiation (UV) exposure: Friends and foes to the skin and beyond the skin. *Environ Int*. 2024;185:108535. https://doi.org/10.1016/j.envint.2024.108535.
36 Ansary TM, Hossain MR, Kamiya K, et al. Inflammatory molecules associated with ultraviolet radiation-mediated skin aging. *Int J Mol Sci*. 2021;22:3974. https://doi.org/10.3390/ijms22083974.
37 Heck DE, Vetrano AM, Mariano TM, et al. UVB light stimulates production of reactive oxygen species: unexpected role for catalase. *J Biol Chem*. 2003;278:22432-22436. https://doi.org/10.1074/jbc.C300048200.
38 Chen HY, Lin CH, Wu Y, et al. Protective effects of degraded *Bletilla striata* polysaccharides against UVB-induced oxidative stress in skin. *Int J Biol Macromol*. 2024;277:134462. https://doi.org/10.1016/j.ijbiomac.2024.134462.

39 Kim SH, Lee SE, Kim SJ, et al. Protective effects of an electrophilic metabolite of docosahexaenoic acid on UVB-induced oxidative cell death, dermatitis, and carcinogenesis. *Redox Biol*. 2023;62:102666. https://doi.org/10.1016/j.redox.2023.102666.

40 Lei Yl, Wang K, Deng Lf, et al. Redox regulation of inflammation: old elements, a new story. *Med Res Rev*. 2015;35:306-340. https://doi.org/10.1002/med.21330.

41 Chen WQ, Kang J, Xia JP, et al. p53-related apoptosis resistance and tumor suppression activity in UVB-induced premature senescent human skin fibroblasts. *Int J Mol Med*. 2008;21:645-653. https://doi.org/10.3892/ijmm.21.5.645.

42 Tang XW, Zhu YC, Han LD, et al. CP-31398 restores mutant p53 tumor suppressor function and inhibits UVB-induced skin carcinogenesis in mice. *J Clin Invest*. 2007;117:3753-3764. https://doi.org/10.1172/jci32481.

43 Nagase H, Visse R, Murphy G. Structure and function of matrix metalloproteinases and TIMPs. *Cardiovasc Res*. 2006;69:562-573. https://doi.org/10.1016/j.cardiores.2005.12.002.

44 Kim C, Ryu HC, Kim JH. Low-dose UVB irradiation stimulates matrix metalloproteinase-1 expression *via* a BLT2-linked pathway in HaCaT cells. *Exp Mol Med*. 2010;42:833-841. https://doi.org/10.3858/emm.2010.42.12.086.

45 Mizushima N, Levine B. Autophagy in human diseases. *N Engl J Med*. 2020;383:1564-1576. https://doi.org/10.1056/NEJMra2022774.

46 Ravikumar B, Sarkar S, Davies JE, et al. Regulation of mammalian autophagy in physiology and pathophysiology. *Physiol Rev*. 2010;90:1383-1435. https://doi.org/10.1152/physrev.00030.2009.

47 Zou L, Liao MR, Zhen YQ, et al. Autophagy and beyond: Unraveling the complexity of UNC-51-like kinase 1 (ULK1) from biological functions to therapeutic implications. *Acta Pharm Sin B*. 2022;12:3743-3782. https://doi.org/10.1016/j.apsb.2022.06.004.

48 Codogno P, Mehrpour M, Proikas-Cezanne T. Canonical and non-canonical autophagy: variations on a common theme of self-eating? *Nat Rev Mol Cell Biol*. 2011;13:7-12.https://doi.org/10.1038/nrm3249

49 Ke J, Wang J, Wu X, et al. Salidroside ameliorates ultraviolet-induced keratinocyte injury by inducing SIRT1-dependent autophagy. *Clin Cosmet Investig Dermatol*. 2022;15:1499-1508. https://doi.org/10.2147/ccid.S367233.

50 Egan DF, Shackelford DB, Mihaylova MM, et al. Phosphorylation of ULK1 (hATG1) by AMP-activated protein kinase connects energy sensing to mitophagy. *Science*. 2011;331:456-461. https://doi.org/10.1126/science.1196371.

51 Herzig S, Shaw RJ. AMPK: guardian of metabolism and mitochondrial homeostasis. *Nat Rev Mol Cell Biol*. 2018;19:121-135. https://doi.org/10.1038/nrm.2017.95.

52 Matsuzawa-Ishimoto Y, Hwang S, Cadwell K. Autophagy and inflammation. *Annu Rev Immunol*. 2018;36:73-101. https://doi.org/10.1146/annurev-immunol-042617-053253.

53 Du JF, Xu Q, Zhao H, et al. PI3K inhibitor 3-MA promotes the antiproliferative activity of esomeprazole in gastric cancer cells by downregulating EGFR *via* the PI3K/FOXO3a pathway. *Biomed Pharmacother*. 2022;148:112665. https://doi.org/10.1016/j.biopha.2022.112665.